[3] Szegedy C, Vanhoucke V, Ioffe S, Shlens J, Wojna Z (2015) Rethinking the inception architecture for computer vision. ArXiv preprint: 1512.00567
[4] Yi D, Sawyer R, Cohn III D, Dunnmon J, Lam C, Xiao X, Rubin D (2017) Optimizing and visualizing deep learning for benign/malignant classification in breast tumors. ArXiv preprint: 1705.06362
[5] Setiawan AS, Wesley J, Purnama Y (2015) Mammogram classification using law's texture energy measure and neural networks. Procedia Computer Science 58: 92–97

Radiomics association of MRI texture features with spondyloarthritis and sacroiliitis

A. P. Magalhães Tenorio[1], M. Calil Faleiros[2], J. Raniery Ferreira Junior[2], V. Faeda Dalto[1], R. Luppino Assad[1], H. Yoshida[3], M. H. Nogueira-Barbosa[1], P. M. Azevedo-Marques[1]
[1]University of São Paulo, Ribeirão Preto Medical School, Ribeirão Preto, Brazil
[2]University of São Paulo, São Carlos School of Engineering, São Carlos, Brazil
[3]Harvard Medical School, Massachusetts General Hospital, Boston, United States

Keywords Radiomics · Spondyloarthritis · Sacroiliitis · Quantitative image analysis

Purpose

Spondyloarthritis (SpA) comprises a set of diseases sharing common clinical manifestations, such as inflammatory axial pain, enthesopathies, and peripheral arthritis. The Assessment of Spondyloarthritis International Society (ASAS) Group classification criteria for axial SpA introduced sacroiliac joints active inflammation (sacroiliitis) assessed using Magnetic Resonance Imaging (MRI) as one of the most important criteria in the classification of SpA. Furthermore, therapy decision considers, among other factors, the subtype of the SpA, which makes the diagnosis and subclassification of SpA crucial for treatment [1]. Recently, radiomics has emerged as a promising approach to improve diagnosis and to provide therapy decision support for precision medicine. Radiomics consists of the massive extraction of quantitative features from medical images and their association with clinical outcomes [2]. The main objective of this study is to evaluate the use of radiomics to aid the diagnosis and therapy decision of SpA by associating quantitative MRI texture features with the outcomes of presence of sacroiliitis, diagnosis of SpA, and subclassification in axial or peripheral SpA.

Methods

Our institutional research board approved this retrospective study with a waiver of patients' informed consent. MRI exams of 47 patients were used in this study after anonymization. From each MRI exam, we selected 6 consecutive images in the coronal plane acquired with fluid sensitive technique. Each image was manually segmented by a musculoskeletal radiologist and processed by the warp geometric transform to reduce noise [3]. Texture features were extracted from each MRI image and categorized as: gray-level Histogram, Haralick, Tamura, Fourier, Gabor, Wavelet, and Fractal. Each exam was characterized by the mean and standard deviation of each feature for the 6 images, totalizing 230 features.

Quantitative image features were first assessed univariately by the Mann–Whitney *U* test for the association with presence of sacroiliitis (S+ or S−), diagnosis of SpA (SpA or Other Pathology), and subtype of SpA (Axial or Peripheral). Diagnoses were obtained from patient's records using the ASAS criteria [1, 4]. Quantitative image features were also assessed multivariately by a machine learning model based on the ReliefF feature selection method and an Artificial Neural Network (ANN) [5]. This model finds the highest performance for the combination of x selected features and y ANN neurons, where x varied from 1 to all 230 features and y varied from 1 to the number of samples of the majority outcome group. Association was assessed by the area under the receiver operating characteristic curve (AUC) using the leave-one-out cross-validation method.

Results

The univariate analysis showed that the Tamura_D11_SD feature yielded the highest overall performance in distinguishing the diagnostic outcomes with AUC equal to 0.97 (association with axial SpA and peripheral SpA, $p < 0.0001$). Histogram_Skewness_M feature yielded the highest performance to identify the presence of inflammation in the sacroiliac joints with AUC of 0.86 ($p < 0.0001$). Tamura_D11_SD feature also yielded the highest associative performance in differentiating SpA from other pathologies with AUC of 0.80 ($p < 0.001$) (Table 1).

Table 1 Highest AUC values obtained by the univariate and multivariate analyses

Outcome	Univariate analysis	Multivariate analysis
Sacroiliitis presence (S+ vs. S−)	0.86 (Histogram_ Skewness_M)	0.96 (25 n + 59 f)
SpA diagnosis (SpA vs. other)	0.80 (Tamura_D11_SD)	0.83 (18 n + 32 f)
SpA subtype (Axial vs. peripheral)	0.97 (Tamura_D11_SD)	0.99 (5 n + 26 f)

Feature and number of ANN neurons (n) + number of features (f) that yielded the highest performance are shown in the parentheses

On the other hand, the multivariate analysis, using the ANN and the most relevant attributes (according to the ReliefF method), was able to increase the AUC value by 0.10 units (sacroiliitis presence) as shown in Table 1. However, the AUC values were similar to those of the univariate analysis, especially for SpA subtype with a difference of only 0.02.

Conclusion

MRI analysis to SpA diagnosis may be a difficult task. To potentially improve the diagnosis of these pathologies and their therapy decision, this work applied radiomics techniques by extracting 230 quantitative MRI texture features and associate them with clinical diagnostic outcomes of SpA. Statistical and machine learning analyses were performed to assess the associative performance of the features across the different SpA outcomes.

Histogram_Skewness_M feature presented high association with sacroiliitis presence and Tamura_D11_SD feature with SpA diagnosis and subtypes. In contrast, combining several different quantitative MRI texture features into a machine learning model presented highest associative performance for sacroiliitis and SpA diagnostic outcomes. Several different disease patterns from the Other Pathology group may have interfered with the SpA diagnosis association due to the low AUC values. Further investigation is necessary to improve its associative performance and aid the diagnosis and therapy decision of SpA.

Acknowledgements

We thank CAPES, CNPq, FAPESP, and FAEPA-HCFMRP-USP for financial support.

References

[1] Sieper J, Rudwaleit M, Baraliakos X, Brandt J, Braun J, Burgos-Vargas R et al. (2009) The Assessment of Spondyloarthritis international Society (ASAS) handbook: a guide to assess spondyloarthritis. Annals of the Rheumatic Diseases 68(Suppl 2): ii1-ii44.

[2] Gillies R, Kinahan P, Hricak H (2016) Radiomics: Images Are More than Pictures, They Are Data. Radiology 278(2): 563–77.
[3] Faleiros MC, Ferreira Junior JR, Jens EZ, Dalto VF, Nogueira-Barbosa MH, Azevedo-Marques PM (2018) Pattern Recognition of Inflammatory Sacroiliitis in Magnetic Resonance Imaging. Lecture Notes in Computational Vision and Biomechanics 27: 639–644.
[4] Rudwaleit M, Heijde D, Landewé R, Akkoc N, Brandt J, Chou CT et al. (2011) The Assessment of SpondyloArthritis international Society classification criteria for peripheral spondyloarthritis and for spondyloarthritis in general. Annals of the Rheumatic Diseases 70: 25–31.
[5] Ferreira Junior JR, Cipriano F, Fabro A, Koenigkam-Santos M, Azevedo-Marques, PM (2018) Radiomics-based recognition of metastatic and histopathological patterns of lung cancer. Lecture Notes in Computational Vision and Biomechanics 27: 613–623.

Recognition algorithm of anatomical skeleton in a bone scintigram

T. Kanamori[1], A. Saito[1], S. Hanaoka[2], S. Higashiyama[3], J. Kawabe[3], S. Shiomi[3], A. Shimizu[1]
[1]Tokyo University of Agriculture and Technology, Institute of Engineering, Koganei, Japan
[2]The University of Tokyo Hospital, Department of Radiology, Bunkyo, Japan
[3]Osaka City University, Department of Nuclear Medicine, Graduate School of Medicine, Osaka, Japan

Keywords Skeleton · Multi-atlas segmentation · Bone scintigram · Prostate cancer

Purpose

A bone scintigram is effective in detecting bony metastases of prostate cancer [1]. Several papers have proposed computer aided diagnosis (CAD) systems for assisting metastasis detection [2–4], in which precise recognition of an anatomical skeleton is essential for cancer staging. Sadik et al. proposed an algorithm segmenting four skeletons using an active shape model [2]. As the algorithm uses a single model of four skeletons, it might fail in segmentation in a scenario where the skeleton shape differs from the model. Kikuchi et al. [3] presented a method using a nonlinearly deformed skeleton atlas to recognize skeletons of a test case. However, this method, too, suffers from the difference in shape between the atlas and the case with atypical skeleton shape.

This paper proposes a novel method to recognize skeletons in bone scintigrams. The method is multi-atlas based segmentation [5] of multiple bones, in which multiple atlases of 15 bones are used to recognize a skeleton in a scintigram. We apply the proposed method to 103 cases and discuss its effectiveness.

Methods

The inputs are a bone scintigram and a database composed of pairs of a bone scintigram and corresponding manually delineated anatomical labels, named "atlas" in this paper. The proposed algorithm to recognize 15 bones in a bone scintigram is as follows.

Spatial standardization

The algorithm spatially standardizes the input scintigram and those in the database simultaneously. The process consists of three steps: body axis correction, affine transformation, and free-form deformation, to align all scintigrams in the database to the input one.

Deformation of multiple atlases based on the spatial standardization

All anatomical labels in the database were deformed using the results of the spatial standardization.

Removal of hot spots

Given that hot spots with high accumulation make the next atlas matching process fail, we estimated hot spot regions approximately and removed such regions from the input scintigram.

Atlas matching for each bone

All anatomical labels in the database were aligned to the input scintigram. To this end, template matching between the input scintigram and those in the database was employed. The evaluation value used in the template matching was normalized mutual information (NMI). The location with the maximum NMI was identified. The multiple anatomical labels of each bone in the database were transformed based on the template matching. This process works well for large bones, such as a cranial bone and ribs, but fails for small bones, e.g., cervical vertebrae. Therefore, we proposed a conditional template matching for small bones, in which conditional labels are generated based on the results of template matching of neighboring large bones, e.g., a skull for cervical vertebrae.

Probabilistic atlas based recognition

Pixel-wise recognition of an anatomical skeleton was carried out by a weighted majority vote based on the aligned anatomical labels.

Inverse transformation of spatial standardization

Inverse transformation of the spatial standardization was applied to obtain the results corresponding to an original scintigram.

Results

We applied the proposed algorithm to bone scintigrams of 103 cases and evaluated the performance as the Jaccard Index (JI) between a segmented region of each bone and its manually delineated true label. The size of a scintigram is 512 × 1024 pixels and the pixel size is 2.8 mm.

Figure 1 shows an example of skeleton segmentation with true labels of bones. As shown in the subtraction image between the segmentation result and corresponding true labels, the difference is small enough for cancer staging. The average JI of 15 bones in this case was 0.847. Figure 2 presents JIs of 103 cases evaluated by a leave-one-out method. The average was 0.800, which was satisfactory on average, because the inter-observer variation of JIs of true labels was approximately distributed from 0.7 to 0.8. However, the results of several bones, such as scapula and humerus, indicate low JIs, which will be tackled in the near future.

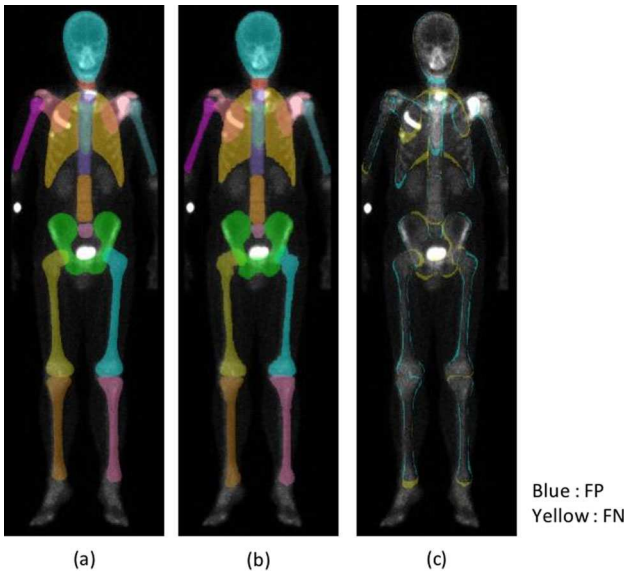

Fig. 1 **a** Segmentation result, **b** true labels, and **c** subtraction image between (**a**) and (**b**)